J Therm Anal Calorim (2016) 126:1007–1013
DOI 10.1007/s10973-016-5674-5

Dilatometry analysis of the sintering process of nanostructured gadolinia-doped ceria

R. M. Batista[1] · E. N. S. Muccillo[1]

Received: 29 March 2016 / Accepted: 29 June 2016 / Published online: 12 July 2016

Abstract The sintering process of compacts of nanostructured gadolinia-doped ceria was investigated by dilatometry and by construction of the master sintering curve. Corrections for the thermal expansion of the experimental setup and mass loss were proposed. The aim of this work was to investigate the sintering evolution of compacts constituted by a powder material with very high specific surface area and to verify the effectiveness of the proposed corrections for generating reliable density data. Validation of the obtained results was accomplished by comparison of corrected data with density values obtained for conventionally sintered compacts. Dilatometry experiments were carried out for 3, 6, 10 and 12 °C min^{-1} heating rates. Good convergence of relative density curves calculated from corrected shrinkage data was obtained. The determined value of the activation energy for sintering of nanostructured gadolinia-doped ceria compacts is 576 kJ mol^{-1}.

Keywords TG · DRX · Ceria · Dilatometry · Sintering

Introduction

Sintering is one of the most relevant steps in the processing of ceramic powders. It is a thermodynamic process that yields changes in the microstructure and properties of ceramic compacts and accounts for their mechanical strength, final microstructure, and macroscopic properties [1, 2]. Improvements in the microstructure control along with other technological issues have been the focus of recent studies [3].

Several experimental techniques have been used to characterize the sintering process, especially the thermodilatometry, or simply dilatometry. This technique allows for studying the kinetics of sintering by measuring dimensional changes in ceramic compacts subjected to a preset heating–cooling cycle [4–7]. Sometimes, results obtained by dilatometry are utilized for constructing sintering maps and the so-called master sintering curve MSC [7] allowing for predicting the sintering behavior of the investigated material.

It is common practice to manipulate dilatometry data according to the ASTM EE228-11 that standardizes procedures for thermal expansion determination of materials using a push-rod dilatometer [8]. In the study of shrinkage of powder compacts, some corrections are worth to be introduced to avoid systematic errors. Some corrections of dilatometry data may be found in the literature [4, 9–13], the most usual being for thermal expansion of the sample material.

The formalism of MSC has been applied to study the sintering kinetics of 10 mol % Gd_2O_3-doped CeO_2 (GDC) solid electrolyte, for powders with specific surface areas up to $\sim$50 m^2 g^{-1} [4, 14–16].

In this work, we investigated the sintering process of GDC with very high specific surface area (>200 m^2 g^{-1}) by the construction of the MSC. Special attention was paid to corrections applied to dilatometry data, specifically for the thermal expansion of the specimen and the assembly, and mass loss. The validation of the proposed corrections on the MSC was performed by comparison of the calculated results with density values obtained in conventionally sintered specimens.

✉ E. N. S. Muccillo
enavarro@usp.br

[1] Center of Materials Science and Technology, Energy and Nuclear Research Institute – IPEN, PO Box 11049, São Paulo, SP 05422-970, Brazil

Linear shrinkage and density

In a typical dilatometer experiment, the changes in sample dimension in a single direction are continuously recorded during a heating–cooling cycle. To monitor these changes, a displacement sensor is coupled to the experimental setup. Both the sample holder and the probe are constituted by the same material and exhibit the same thermal expansion. Then, the displacement measured, ΔL_m, at each temperature by a linear variable differential transducer (LVDT) consists of two contributions: the dimensional change in the sample, ΔL_s, and the thermal expansion of the assembly, ΔL_a, (sample holder plus probe). This may be represented by Eq. (1):

$$\Delta L_m = \Delta L_s - \Delta L_a \tag{1}$$

Several phenomena may induce dimensional changes in a ceramic material such as its thermal expansion, the linear shrinkage that occurs during heating, the mass loss due to adsorbed organic species or thermal decomposition of the material and phase transitions [17, 18]. The mass loss becomes relevant whenever the powder has a high specific surface area. This effect is particularly significant in chemically synthesized ceramic powders if the decomposition reaction of the precursor material is somehow incomplete, as for example, for a too low calcination temperature, and then, the sintering is accompanied by mass loss due to the decomposition reaction.

Assuming that there are no phase transitions or decomposition reactions, and the mass loss is negligible during the thermal cycle, Eq. (1) may be rewritten as:

$$\Delta L_m = \Delta L_{sinter} + \Delta L_{TE} - \Delta L_a \tag{2}$$

where ΔL_{sinter} is the total displacement produced by sintering the powder compact, and ΔL_{TE} the displacement induced by the thermal expansion of the powder material. In general, the main goal in sintering experiments is to determine the linear shrinkage term due to the sintering process. This term allows for applying the theoretical models to experimental data and to preview the total linear shrinkage of the sample.

To determine ΔL_{sinter}, we define the variables: L_0' and L', given by:

$$L_0' = L_0 + \Delta L_{sinter} \tag{3}$$

and

$$L' = L_0' + \Delta L_{TE} \tag{4}$$

In these equations, L_0' represents the length of the compact if the dilatometry run is interrupted at any temperature and the compact is conducted to the initial temperature, and L' is the instantaneous length of the compact at a time t.

The displacement term in Eq. (2) may be determined by the analysis of a standard sample with well-known thermal expansion. Then, a correction function F_c may be determined according to the procedure suggested in [8, 19]. After manipulation of previous equations, ΔL_a is given by:

$$\Delta L_a = F_c \cdot (L_0 + \Delta L_{sinter}) \tag{5}$$

The displacement due to thermal expansion of the sample is:

$$\Delta L_{TE} = (L_0 \cdot F_E + \Delta L_{sinter} \cdot F_E) \tag{6}$$

where F_E is a function that quantifies the thermal expansion of the sample at each temperature. This function may be experimentally determined by the analysis of the linear shrinkage curve during cooling down to room temperature the studied sample or by measuring an already sintered sample.

It is worth noting that both terms related to the thermal expansion, ΔL_s and ΔL_a, depend on the shrinkage. Substituting (2), (5) and (6) in (1) and rearranging results:

$$\frac{\Delta L_{sinter}}{L_0} = \left(\frac{\Delta L_m}{L_0} + F_c - F_E\right) \cdot \left(\frac{1}{1 + F_E - F_c}\right) \tag{7}$$

This equation was used for calculating the linear shrinkage of the powder compacts.

The density, ρ, of the compact may be determined from the linear shrinkage data. Assuming isotropic shrinkage and negligible mass loss, the density is usually calculated from [2]:

$$\rho = \frac{\rho_0}{\left(1 + \frac{\Delta L_{sinter}}{L_0}\right)^3} \tag{8}$$

where ρ_0 is the green density.

Whenever the mass loss may not be neglected, a correction function f(t,T) should be determined from thermogravimetry results. This function establishes the ratio of the initial mass to that at any temperature. In this case, Eq. (8) is modified to:

$$\rho = \frac{\rho_{0 \cdot f(t,T)}}{\left(1 + \frac{\Delta L_{sinter}}{L_0}\right)^3} \tag{9}$$

These corrections, Eqs. (7) and (9), are proposed to increase the overall precision in the analysis of dilatometry data.

Experimental

Specimen preparation

Nanostructured $Ce_{0.9}Gd_{0.1}O_{2-\delta}$, GDC (99.5 %, Fuel Cell Materials, USA), with specific surface area of 210 $m^2\ g^{-1}$

was used as starting material. No additives were employed during processing, and the powder was carefully handled to avoid contamination.

Disk-shaped specimens with 5 mm diameter and 12–16 mm thickness for dilatometry and with 10 mm diameter and 2–3 mm thickness for conventional sintering experiments were prepared by uniaxial pressing with 50 MPa followed by cold isostatic pressing (National Forge Co) at 70 MPa. Sintering of the green compacts in powder bed was carried out by the conventional method in a resistive furnace (Lindberg BlueM) with 10 °C min^{-1} heating rate at dwell temperatures from 600 to 1400 °C and holding times of 0–15 h (Note: 0 stands for no holding time meaning that the specimen was cooled down to room temperature as soon as the sintering temperature was attained).

Dilatometry and data analysis

Dilatometry experiments were conducted in a push-rod vertical dilatometer (Anter, Unitherm™ 1161) for monitoring the in situ shrinkage of the sample in air up to 1400 °C with heating rates of 3, 6, 10 and 12 °C min^{-1} and cooling rate of 10 °C min^{-1}. In these measurements, the specimens were first heated to 600 °C remaining for 10 min for elimination of adsorbed species and then heated up to the maximum temperature. The temperature near the compact was measured by an S-type thermocouple. Displacement measurements were performed by a LVDT sensor with nominal precision of 0.001 mm. The thermal expansion of the setup was evaluated by measuring a translucent alumina Crystalox® as reference material. The thermal expansion of GDC specimen was corrected from the observed shrinkage using the values corresponding to the thermal expansion coefficient determined from the slope of the shrinkage–straight line recorded in the cooling process.

Dilatometry data were analyzed by software specially designed for constructing the MSC. Details of the software will be the subject of a future publication. In the MSC model, the instantaneous density is plotted as a function of the work of sintering, $\Theta(t,T(t))$, given by [7]:

$$\Theta(t,T(t)) = \int_0^t \frac{1}{T}\exp\left(-\frac{Q}{RT}\right)\mathrm{d}t \qquad (10)$$

where Q is the apparent activation energy for sintering, T the absolute temperature, R the gas constant, and t the time.

Integration of Eq. (10) is straightforward whenever the value of Q is known. Nevertheless, in most cases that value is unknown. Initially, the form of the density curve is assumed to be represented by a polynomial or a sigmoid function. Then, for numerical construction of MSC, the density curves are converted to density versus $\Theta(t,T(t))$ curves with pre-assumed value of Q. This procedure is repeated a number of times, and the results are plotted as mean residual squares versus Q. When the correct value of Q is chosen, the diverse density curves converge to a single one. The convergence of the data is quantified by the sum of the residual squares of the points with respect to the fitted line. Then, the best value of Q corresponds to that minimizing the obtained mean residual square values. Full description of this procedure may be found elsewhere [7]. In this case, the density curve was represented by a sigmoid function.

Characterization methods

The primary particle size of GDC was estimated by transmission electron microscopy, TEM (Jeol, JEM 2100), images analyzed with the ImageJ software. The mean crystallite size was determined by X-ray diffraction experiment, XRD (Bruker-AXS, D8 Advance) with Cu K_α radiation in the 23–73° 2θ range, 0.04° step size and 5 s per step counting time. The analysis of the XRD pattern was performed by Rietveld method using GSAS [20]. The mass loss was quantified by thermogravimetry, TG (Netzsch, STA 409E), and the organic impurities were determined by mass spectrometry (Thermostar, GSD320) coupled to the thermal analysis setup. The thermal analyses were carried out up to 1300 °C in alumina crucibles and atmosphere of synthetic air or nitrogen (5 mL min^{-1}) with heating rate of 10 °C min^{-1}. The green and the sintered densities of GDC specimens were calculated from the measurements of sample mass (Mettler H315) and dimensions (micrometer Tesa, CH-1020).

Results and discussion

Powder characterization

Figure 1 shows a representative TEM micrograph of GDC powder consisting of polygonal-shaped nanostructured particles, with narrow distribution in size and some degree of agglomeration. The calculated mean primary particle size is 3.3 nm.

Figure 2 shows the XRD pattern of GDC powder with the Rietveld refinement. Small crosses in the bottom of this figure are the Bragg angular position of the cubic phase (*Fm-3m*, space group) reflections. The value of Chi-square was 1.05. The experimental pattern corresponds to the characteristic cubic fluorite-like phase of ceria, and the mean crystallite size is 4.2 nm, in agreement with the mean primary particle size obtained by TEM. Other parameters calculated from the XRD pattern are the microstrain, which is negligible (5×10^{-4} %), and the theoretical density 7.21 g cm^{-3}.

The mean particle size calculated from the specific surface area assuming a spherical shape of the powder particles is 5.3 nm. These results on primary particle, crystallite and particle sizes reveal that the starting material consists of single-crystalline nanoparticles, within the resolution limits and experimental precision of the diverse techniques.

Figure 3a shows the TG curve of GDC powder up to 1300 °C. Most of the mass loss (~8 %) occurs up to 200 °C, although it is negligible only above 600 °C. The total mass loss is 13 %.

It is generally known that physisorbed water may account for the mass loss up to approximately 200 °C. The origin of the mass loss occurring at higher temperatures was investigated by mass spectrometry up to 400 °C. Figure 3b shows mass spectrometry results obtained at 100, 290 and 400 °C.

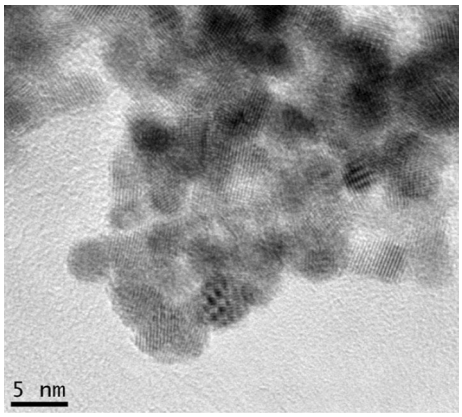

Fig. 1 Bright-field TEM micrograph of nanostructured GDC powder

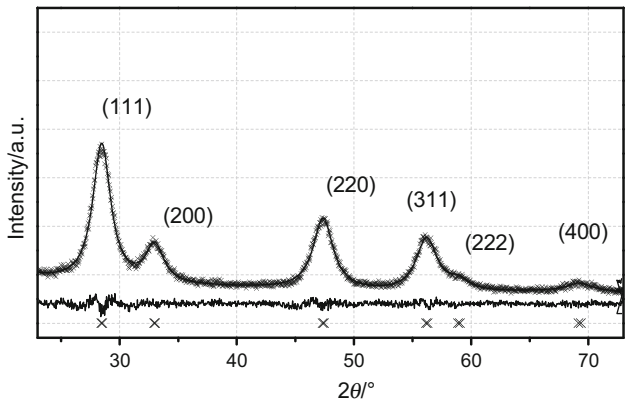

Fig. 2 XRD pattern of GDC powder. Experimental data (*small crosses*), Rietveld refinement (*line*), residues (*line* below XRD pattern) and angular position of the cubic fluorite-like reflections (*crosses* at the *bottom*)

Signals due to OH, O_2, CO and CO_2 along with water are identified in these spectra. The signals corresponding to N_2 come from the flowing gas during this analysis. These results evidence that organic impurities from the surrounding atmosphere had been adsorbed onto particles surface, probably during sample manipulation. This effect is significant in this case, due to the very high specific surface area of GDC powder.

Densification and MSC

The relative green density of powder compacts is low, about 40 %, as expected for nanostructured powders.

Several compacts were sintered by the conventional method to assure the isotropic character of the GDC shrinkage. The results are shown in Fig. 4.

The linear shrinkage is approximately the same in axial and radial directions and, therefore, the densification is isotropic in GDC.

Figure 5 shows linear shrinkage curves of GDC compacts obtained with 10 °C min^{-1} heating rate after

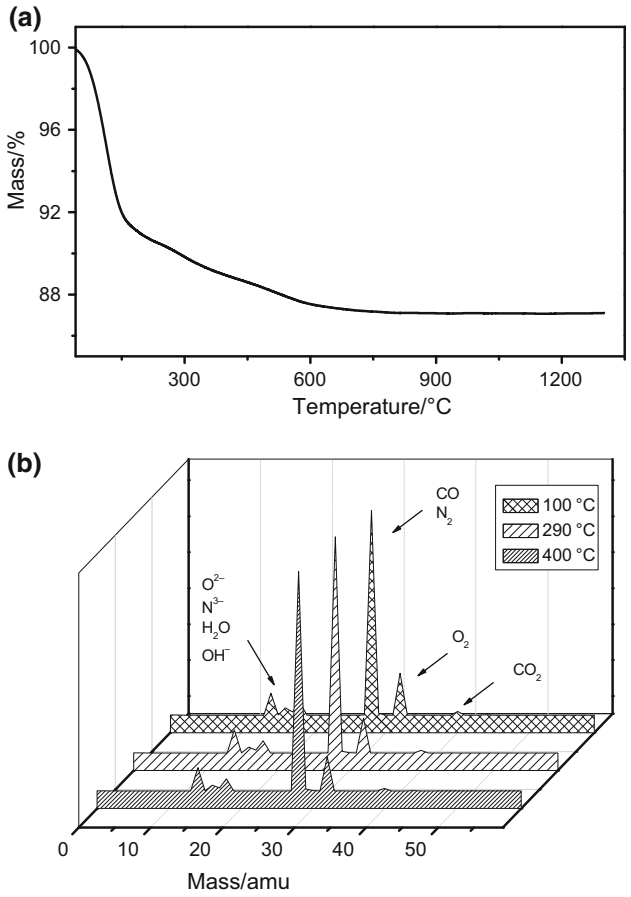

Fig. 3 **a** TG curve and **b** mass spectrometry spectra of GDC nanostructured powder obtained at 100, 290 and 400 °C

correction of the experimental data for thermal expansion according to ASTM E228-11 standard and Eq. (7).

The shrinkage finishes at approximately 1200 °C, and the total shrinkage is about 30 %. The compact starts to shrink at relatively low temperatures due to the combined effects of small particle size and mass loss (Fig. 3a). The onset temperature of linear shrinkage, however, may not be precisely determined. The main difference between the use of ASTM standard and Eq. (7) occurs at high temperatures amounting 2 %.

The influence of corrections for thermal expansion and mass loss on density curve of GDC is exemplified in Fig. 6 for data obtained with 10 °C min^{-1} heating rate.

Continuous lines represent the calculated data with and without corrections. Relatively low density values are generated when the thermal expansion contribution is not taken into account. The influence of mass loss is even more severe resulting in unreasonably higher density values. This last effect is better seen at high temperatures.

The discrete points were obtained for GDC compacts sintered by the conventional method, and that near the origin is the green density. The excellent agreement between the continuous line representing the corrected experimental data and the discrete density values validates the proposed methodology for data correction.

Figure 7 shows density curves of GDC compacts obtained from corrected linear shrinkage data measured for several heating rates. In this case, both Eqs. (7) and (10) were applied to the experimental data.

It may be noted that the density values at any temperature exhibit a slight but systematic dependence on the heating rate, such that the lower is the heating rate, the higher is the relative density. The same effect has been observed in other ceramic materials, like ZnO [7] and Al_2O_3 [21].

The density curves of Fig. 7 were used to calculate the MSC of nanostructured GDC assuming a sigmoid function, and the results are shown in Fig. 8.

The MSC was constructed for a wide range of $\log\Theta$ (Fig. 8a). The determined Q is 576 kJ mol^{-1}. Deviation of the MSC curve from the expected behavior at low and high $\log\Theta$ values may be a consequence of more than one mechanism acting simultaneously in specific ranges of density. The discrete points obtained for conventionally sintered

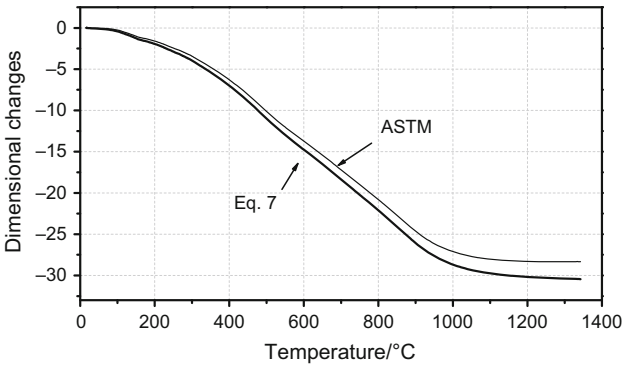

Fig. 5 Linear shrinkage of GDC compact with applied corrections for thermal expansion (heating rate = 10 °C min^{-1})

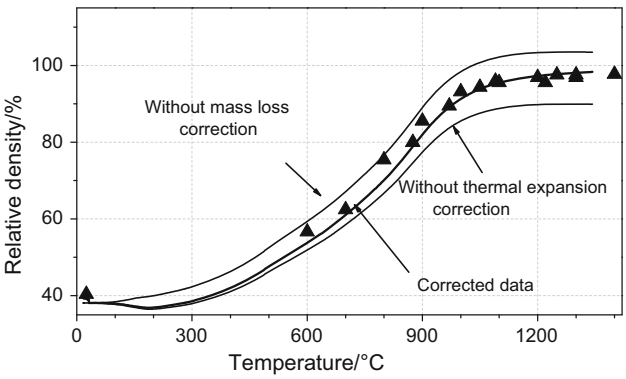

Fig. 6 Relative density of GDC compact with and without corrections for thermal expansion and mass loss (heating rate = 10 °C min^{-1}). Discrete points: values obtained for conventionally sintered specimens

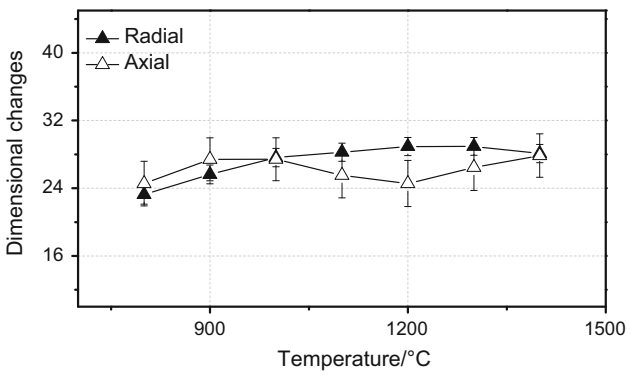

Fig. 4 Linear shrinkage of conventionally sintered GDC compacts measured in axial and radial directions versus sintering temperature

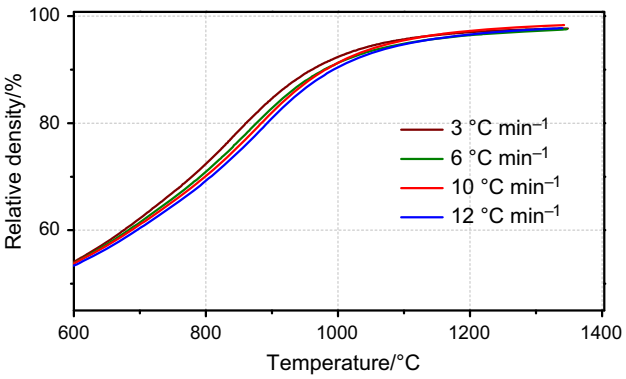

Fig. 7 Relative density versus temperature curves calculated from corrected shrinkage data of GDC compacts at several heating rates

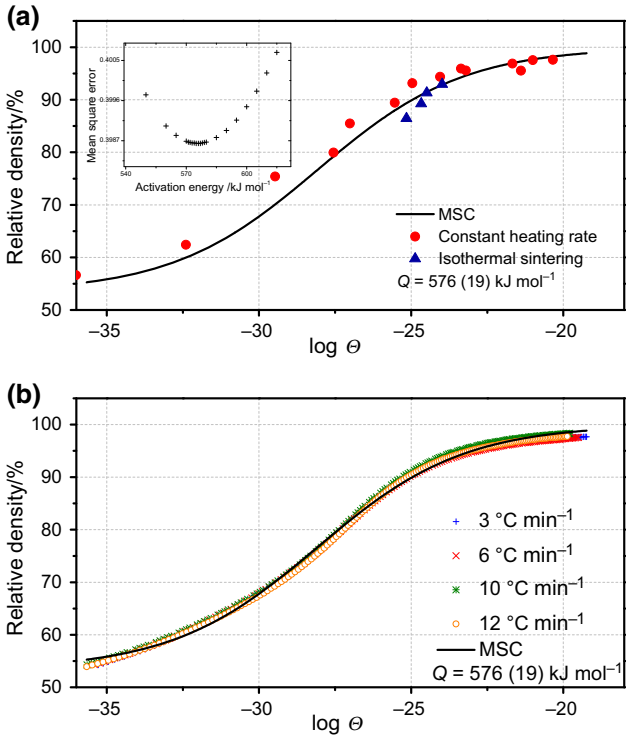

Fig. 8 **a** MSC curve of GDC. Discrete points: density data obtained for conventionally sintered specimens. *Inset* mean of residual squares versus activation energy; **a** convergence of density data for GDC sintered at several heating rates using $Q = 576$ kJ mol^{-1}

GDC compacts validate the MSC formalism with the proposed corrections. The inset shows the dependence of mean residual squares on activation energy values. The Q value determined for nanostructured GDC is consistent, within the experimental precision (± 40 kJ mol^{-1}) with those previously obtained by dilatometry analysis (579 kJ mol^{-1} [14]) and by electrical conductivity (610 kJ mol^{-1} [22]).

Good convergence of density curves (Fig. 8b) was obtained for the determined apparent activation energy value, which is a further evidence of the reliability of the method.

The overall results support that the proposed corrections for linear shrinkage are valuable for manipulating dilatometry data obtained for nanostructured ceramics, especially for sintering studies. Moreover, they reveal that the activation energy for sintering of nanostructured GDC is close to those of powders with moderate values (up to 50 m^2 g^{-1}) of specific surface area.

Conclusions

Nanostructured GDC powder shows a non-negligible mass loss up to approximately 600 °C. Green compacts prepared with this powder exhibit low green density. The linear shrinkage of nanostructured GDC compacts was shown to possess isotropic character. Corrections for linear shrinkage data were proposed for thermal expansion of the assembly and mass loss. From corrected linear shrinkage data, the MSC was determined for nanostructured GDC. The determined value of the activation energy is in fair agreement with previous reports. The MSC curve of GDC was validated by results obtained for conventionally sintered specimens.

Acknowledgements The authors gratefully acknowledge FAPESP (Proc. n°. 2013/07296-2), CNPq (Proc. no. 304073/2014-8) and CNEN for financial supports, and to S. G. M. Carvalho and R. L. Grosso for mass spectrometry analyses. One of the authors (R.M.B.) acknowledges CAPES for the scholarship.

References

1. German RM. Sintering: from empirical observations to scientific principles. Oxford: Elsevier; 2014.
2. Kang SL. Densification, grain growth, and microstructure. Oxford: Elsevier; 2005.
3. Fang ZZ. Sintering of advanced materials. Cambridge: Woodhead; 2010.
4. He Z, Yuan H, Glasscock JA, Chatzichristodoulou C, Phair JW, Kaiser A, Ramousse S. Densification and grain growth during early-stage sintering of $Ce_{0.9}Gd_{0.1}O_{1.95}$-δ in a reducing atmosphere. Acta Mater. 2010;58:3860–6.
5. Pouchly V, Maca K, Shen Z. Two-stage master sintering curve applied to two-step sintering of oxide ceramics. J Eur Ceram Soc. 2013;33:2275–83.
6. Muccillo R, Muccillo ENS. An experimental setup for shrinkage evaluation during electric field-assisted flash sintering: application to yttria-stabilized zirconia. J Eur Ceram Soc. 2013;33:515–20.
7. Su H, Johnson DL. Master sintering curve: a practical approach to sintering. J Am Ceram Soc. 1996;79:3211–7.
8. American Society for Testing Materials, ASTM E228-11. Standard test method for linear thermal expansion of solid materials with a push-rod dilatometer. West Conshohocken: ASTM; 2011.
9. Mazaheri M, Simchi A, Dourandish M, Golestani-Fard F. Master sintering curves of a nanoscale 3Y-TZP powder compacts. Ceram Int. 2009;35:547–54.
10. Maca K, Pouchly V, Boccaccini AR. Sintering densification curve—a practical approach for its construction from dilatometric shrinkage data. Sci Sinter. 2008;40:117–22.
11. Panigrahi BB. Evaluation of dimensional changes from as received dilatometric sintering plot. J Mater Sci Technol. 2007;23:103–7.
12. Blaine DC, Park S, German RM. Linearization of master sintering curve. J Am Ceram Soc. 2009;92:1403–7.
13. Mohapatra G, Sommer F, Mittmeijer EJ. A temperature correction procedure for temperature in homogeneity in dilatometer specimens. Termochim Acta. 2007;453:57–66.
14. Jud E, Huwiler CB, Gauckler LJ. Sintering analysis of undoped and cobalt oxide doped ceria solid solutions. J Am Ceram Soc. 2005;88:3013–9.
15. De Florio DZ, Esposito V, Traversa E, Muccillo R, Fonseca FC. Master sintering curve for Gd-doped CeO_2 solid electrolytes. J Therm Anal Calorim. 2009;97:143–7.
16. Guan L, Le S, He S, Zhu X, Liu T, Sun K. Densification behavior and space charge blocking effect of Bi_2O_3 and Gd_2O_3 co-doped CeO_2 as electrolyte for solid oxide fuel cells. Electrochim Acta. 2015;161:129–36.

17. Ravat B, Oudot B, Perron A, Lalire F, Delaunay F. Phase transformations in PuGa 1 at% alloy: study of whole reversion process following martensitic transformation. J Alloys Compd. 2013;580:298–309.
18. Hillman SH, German RM. Constant heating rate analysis of simultaneous sintering mechanisms in alumina. J Mater Sci. 1992;27:2641–8.
19. Valentich J. Calibration of tube type dilatometers. J Therm Anal Calorim. 1977;11:387–403.
20. Larson AC, von Deele RB. General structure analysis system (GSAS). Los Alamos National Laboratory Report LAUR 86-748; 1994.
21. Ewsuk KG, Ellerby DT, DiAntonio CB. Analysis of nanocrystalline and microcrystalline ZnO sintering using master sintering curves. J Am Ceram Soc. 2006;89:2003–9.
22. Reis SL, Souza ECC, Muccillo ENS. Solid solution formation, densification and ionic conductivity of Gd- and Sm-doped ceria. Solid State Ionics. 2011;192:172–5.